Normal mode paths for hydrogen exchange in the peptide ferrichrome

(peptide surface accessibility/atomic fluctuations)

ROBERT P. SHERIDAN*†, RONALD M. LEVY*‡, AND S. W. ENGLANDER§

*Department of Chemistry, Rutgers University, New Brunswick, New Jersey 08903; and §Department of Biochemistry and Biophysics, University of Pennsylvania, Philadelphia, Pennsylvania 19104

ABSTRACT   Possible paths for exposure to solvent and hydrogen exchange of the amide protons of ferrichrome, a cyclic hexapeptide, are examined. The paths are obtained from calculations of the vibrational normal modes of ferrichrome and correspond to low energy atomic displacements away from the local minimum in the multidimensional conformational space of the molecule. Exposure of exchangeable groups along the normal modes was determined by using the solvent accessible surface area algorithm of Lee and Richards. Three of the exchangeable protons (Gly^{1,2,3}) are largely exposed to solvent in the x-ray structure while the remaining three exchangeable protons of the ornithines are totally shielded from solvent. A very small number of normal mode displacements are found to expose the Orn^2 and Orn^3 amide groups while the Orn^1 amide proton remains shielded from solvent for all the paths studied. The effective paths for exposure of Orn^2 and Orn^3 correspond to the lowest frequency (≈ 18 cm^{-1}) motions. The paths are characterized in terms of the magnitude and energy of atomic displacements, correlated changes in dihedral angles, and the resulting changes in exposure and hydrogen bonding of exchangeable groups.

Hydrogen exchange experiments have been used to probe the dynamics of a wide variety of biopolymers (1–4). However, there is still much uncertainty concerning a molecular interpretation of the experimental results (5–9). Attention is currently focused on two models for hydrogen exchange. One emphasizes the need for cooperative hydrogen bond breakage, which is suggested to occur via individual concerted unfoldings of small molecular segments. Alternatively, penetration models focus on diffusion of hydrogen exchange catalysts into the protein, utilizing multiple small structural fluctuations. There are other possible exchange mechanisms. In this communication we investigate paths for hydrogen exchange in the cyclic hexapeptide ferrichrome. The paths, which are obtained from calculations of the vibrational normal modes of ferrichrome, are characterized in terms of the magnitude and energy of atomic displacements and correlated changes in dihedral angles and the resulting changes in exposure and hydrogen bonding of exchangeable groups.

The cyclic hexapeptide [Gly^3-Gly^2-Gly^1-Orn^3-Orn^2-Orn^1] forms unusually stable and rigid complexes with metal ions. The rigid structure of the metal–peptide complex results in excellent NMR spectroscopic resolution of the six amide hydrogens and the temperature and pH dependence of the amide hydrogen exchange rates have been measured (10–12). The structure of ferrichrome is illustrated in Fig. 1. The peptide backbone forms a type II β turn and the modified ornithyl side chains provide octahedral coordination of the iron. The amide protons of Gly-1 and -2 are completely exposed to solvent and exchange

rapidly with solvent protons. The remaining amide protons are partly or wholly shielded from solvent by other peptide atoms and display slower exchange. One would like to systematically characterize the collective low frequency motions that can lead to increased exposure of the shielded protons. Here we introduce a vibrational normal mode analysis of this problem.

Normal mode studies of molecular motion provide a powerful approach for studying the details of peptide motions in the region of the equilibrium conformation (13–16). Given the local minimum energy geometry, the normal modes are obtained from the solution of the secular equation. The eigenvalues of the secular equation correspond to normal mode frequencies ω_i, with associated eigenvectors Q_i; the components of Q_i give relative amplitudes of the contributing mass-weighted atomic displacements. These eigenvectors can be used to identify low energy paths away from the local minimum in the multidimensional conformational space of the molecule. The paths involve collective displacements of many atoms and a description of them is not readily obtained from molecular model building alone.

METHODS

For the ferrichrome study all atoms were treated explicitly, except CH, CH$_2$, and CH$_3$ groups, which were treated as extended atoms (14); the model contained 55 atoms. The empirical potential function employed has been described previously (17). The starting point for the analysis is a local minimum energy conformation. The x-ray structure of Van der Helm *et al.* (18) was energy minimized by 50 steepest descent steps followed by 50 Newton–Raphson steps. At convergence the minimum energy conformation deviated from the x-ray structure by $\overline{(\Delta r)^2}^{1/2} = 0.63$ Å. Backbone dihedral angles at the equilibrium geometry are presented in Table 1 and hydrogen bond geometries in Table 2. The two strong hydrogen bonds (Orn^{2}H$\cdots$Oζ Orn^2, Orn^{3}H$\cdots$O Gly^3) and the weak hydrogen bond (Gly^{3}H$\cdots$Orn^{3}O) have been identified (10, 11). In the energy minimized conformation, Orn^1 is H-bonded to Oζ of Orn^3. Because there is experimental uncertainty regarding this hydrogen bond, our analysis was carried out both with and without this hydrogen bond initially present, with very similar results; the Orn^{1}H$\cdots$Oζ Orn^3 hydrogen bond was retained in the conformational analysis presented below.

The normal mode analysis of vibrational motion about the minimum energy conformation produced 159 eigenvectors with frequencies between 18 cm and 3,400 cm^{-1}. To identify low energy paths for H exchange, a set of structures corresponding to motion along normal coordinates was generated by adding

† Present address: Lederle Laboratories, Pearl River, NY 10965.
‡ To whom reprint requests should be addressed.
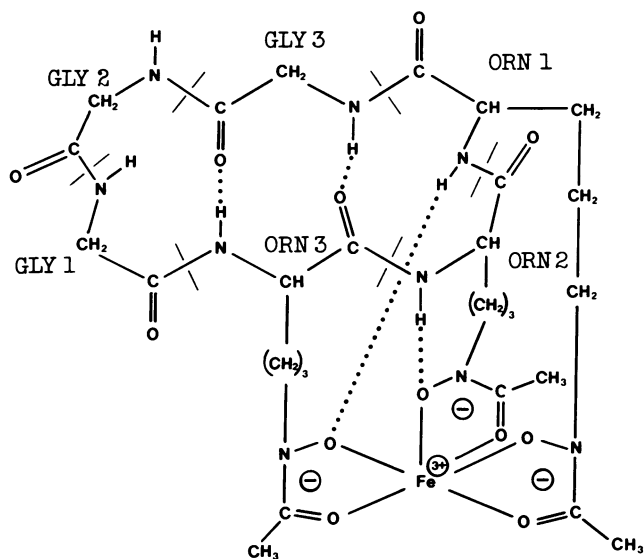
FIG. 1. Schematic diagram of ferrichrome structure. The four hydrogen bonds in the energy minimized structure are indicated by $\cdots$.

normal coordinate displacement vectors to the minimum energy coordinates:

$$\vec{X}_i^\pm = \vec{X}_{min} \pm \sqrt{\frac{E_t}{\omega_i}}\, \vec{Q}_i. \qquad [1]$$

Here $\vec{X}_{min}$ is the minimum energy ferrichrome conformation,

Q_i is the ith normal coordinate eigenvector, and $\vec{X}_i^\pm$ is the ferrichrome conformation distorted along the positive and negative directions of the ith normal mode. The scale factor $\sqrt{E_t/\omega_i}$ normalizes displacements to the same total harmonic strain energy, E_t per mode, so that it is possible to compare the effectiveness with which different modes expose shielded protons. Relatively large displacements were generated (displacements up to $E_t \approx 23$ kcal/mol were studied) to facilitate computer graphics modeling. Although anharmonicity will affect the time dependence of the motions, the use of information about the curvature of the potential surface at the energy minimum to identify correlated displacements leading to solvent contact represents an important simplification of the multidimensional problem of describing hydrogen exchange. The displacements $\vec{X}_i^\pm$ have been constructed by using eigenvectors expressed both in Cartesian and internal coordinates. The same eigenvectors provide effective paths for solvent exposure, whichever components are considered; however, the distorted conformations are slightly different because the transformation from Cartesian to internal coordinates is nonlinear. The results described below correspond to Cartesian displacements. The final coordinates were refined with 10 cycles of steepest descents energy minimization. The refinement eliminated distorted bonds and bond angles resulting from displacements along Cartesian eigenvectors, while the dihedral angles were essentially unchanged. A detailed comparison of the two methods will be presented elsewhere. Exposure of exchangeable protons along the normal modes of the molecule was determined by using the contact surface area algorithm of Lee and Richards (see ref. 19). For the Van der Waals radii used here, an amide
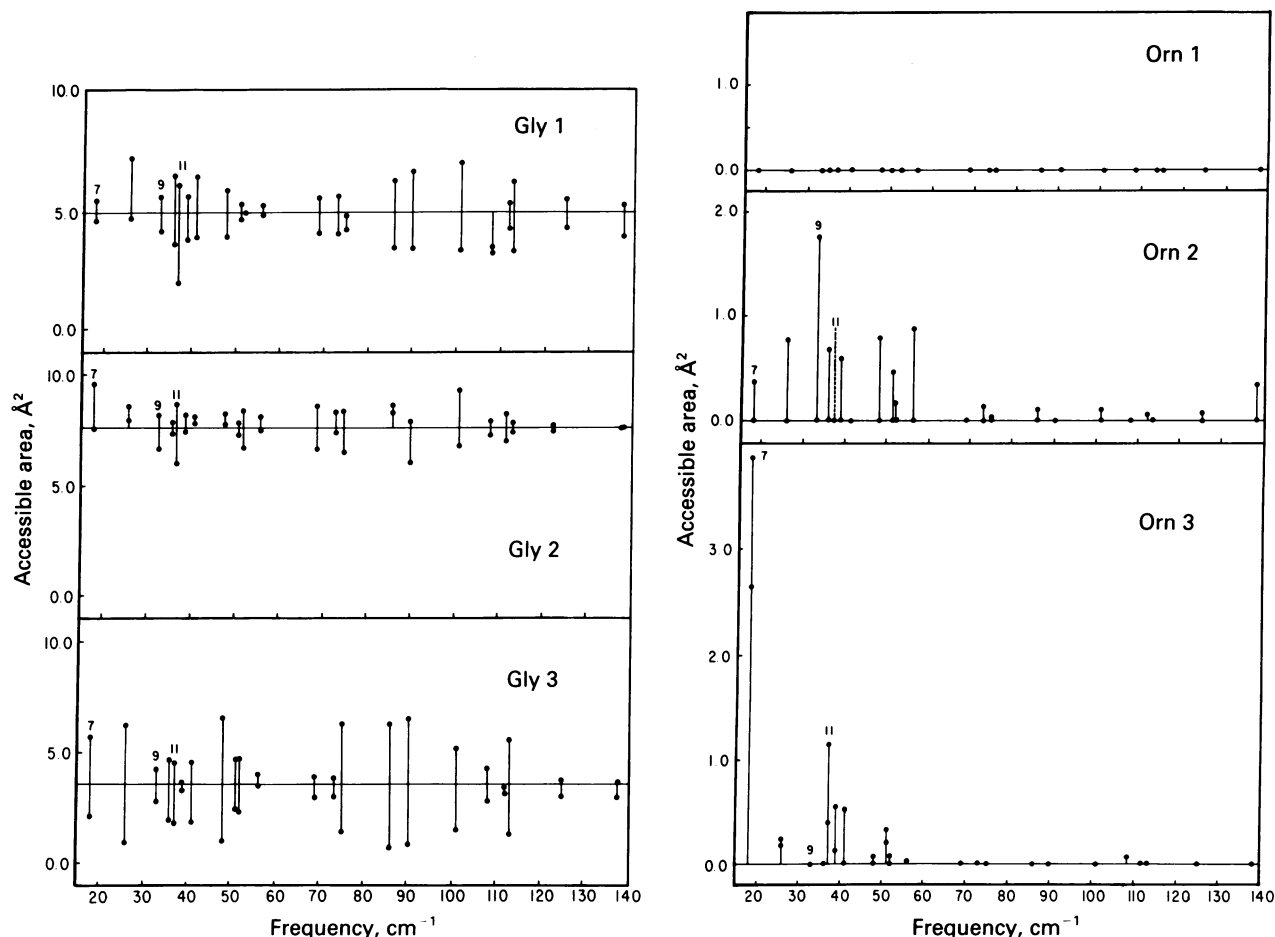
FIG. 2. Accessible surface area of the amide protons along each of the low frequency normal modes. Harmonic strain energy $E = 23$ kcal/mol. The probe radius used in the Lee and Richards algorithm is 1.4 Å. The horizontal line indicates the exposure in the minimum energy structure. Accessible surface area along both X_i^+ and X_i^- are indicated as filled circles. Modes 1–6 (not shown) are rigid body motions.

mode j=   7   9   11
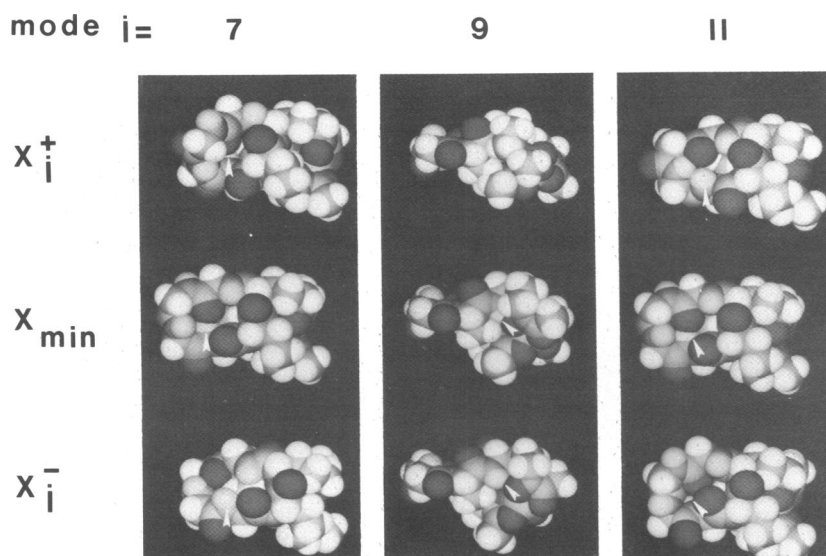
FIG. 3. Space-filling molecular models of the ferrichrome energy minimized conformation and along the exposure paths. Harmonic strain energy E_t = 23 kcal/mol. Front view mode 7 (18 cm^{-1}), which exposes Orn^{3}H; side view mode 9 (33 cm^{-1}), which exposes Orn^{2}H; front view mode 11 (37 cm^{-1}) which exposes Orn^{3}H. The Orn^{2}H and Orn^{3}H protons are indicated by an arrowhead.

proton completely exposed to solvent would have a contact surface area of 10 Å^2. The minimum contact surface area required for hydrogen bonding of a peptide proton to a water molecule is about 0.5 Å^2.

RESULTS AND DISCUSSION

The changes in contact surface area of the six amide protons displaced along each normal mode coordinate are shown in Fig. 2. In contrast to the results for the surface protons (Gly^{1,2,3}), a very small number of normal mode distortions lead to exposure of Orn^2 and Orn^3. The Orn^1 proton is not exposed in any mode for harmonic strain energies up to 23 kcal/mol. The effective paths for exposure of Orn^2 and Orn^3 correspond to the lowest normal mode frequencies. The 18-cm^{-1} mode (mode 7) is the primary path for exposure of the Orn^3 amide proton; an important secondary path occurs at 37 cm^{-1} (mode 11). The major normal mode exposure path for Orn^2 occurs at 33 cm^{-1} (mode 9), although six additional modes appear to contribute. Although the Orn^2 and Orn^3 exposure paths both involve concerted torsional motions, the motions that lead to exchange are very different for the two protons. Pictures of ferrichrome showing exposure of the Orn^{2,3} amide protons along modes 7, 9, and 11 are presented in Fig. 3. The major path for exposure of Orn^{3}H (mode 7) involves "wagging" of the β turn; the proton pokes out above the sheet as the turn bends downward (Fig.

3, X_7^-) and the proton pokes out below the sheet as the turn bends in the opposite direction (Fig. 3, X_7^+). This lowest frequency mode of ferrichrome ruptures the hydrogen bond at the β turn by displacements of donor and acceptor atoms perpendicular to the plane of the turn. The result demonstrates the importance of considering the energetics of fluctuations that can lead to exchange, because on purely geometric grounds it has been suggested that the lowest frequency modes of a β sheet must preserve the hydrogen bonding (20). It is of interest to note that the major path for exposure of Orn^{3}H is not primarily a simple Gly^1-Orn^3 amide plane rock; however, the secondary exchange path does closely correspond to this motion (Fig. 3, $X_{11}^{\pm}$). The path that leads to exposure of Orn^{2}H, mode 9, involves primarily motion of the Orn side chains that form the coordination cage of the Fe while the β sheet structure of the backbone is preserved. For motion along this mode in one direction, the side chain of Orn^2, which in the equilibrium structure shields Orn^{2}H, twists out of the way exposing this proton (Fig. 3). For motion in the opposite direction along this mode Orn^{2}H is completely covered up by the side chain. Atomic displacements and changes in internal coordinates corresponding to the distorted conformations of Fig. 3 are listed in Table 1. With a harmonic strain energy of 23 kcal/mol (the adiabatic total energy will be smaller than this) (14), the rms atomic displacements are 1.5 Å, 0.7 Å, and 0.6 Å for mode 7, mode 9,

Table 1. Hydrogen exchange paths*

	Internal coordinate displacements†																	
	Gly^3			Gly^2			Gly^1			Orn^3			Orn^2			Orn^1		
	ϕ	ψ	ω	ϕ	ψ	ω	ϕ	ψ	ω	ϕ	ψ	ω	ϕ	ψ	ω	ϕ	ψ	ω
Equilibrium	133	160	187	292	107	187	115	341	181	236	213	167	265	320	179	250	76	185
Mode 7 (18 cm^{-1})	12	56	8	8	−34	−8	0	46	39	−35	−18	8	32	−1	−5	−32	−20	−9
Mode 9 (33 cm^{-1})	−12	−13	−4	16	−8	−6	14	−1	3	−8	−15	−4	39	−12	19	−13	15	1
Mode 11 (37 cm^{-1})	−31	−22	−20	64	26	−6	−26	−49	2	33	−41	17	31	7	−5	−10	19	−3

Atomic displacements‡

	Backbone		Side chain		Orn^2		Orn^3	
	Max	Min	Max	Min	N	H	N	H
Mode 7 (18 cm^{-1})	3.9	0.7	1.2	0.3	1.0	1.0	1.1	1.4
Mode 9 (33 cm^{-1})	0.8	0.3	1.3	0.2	0.4	0.8	0.3	0.3
Mode 11 (37 cm^{-1})	1.0	0.1	0.6	0.1	0.2	0.5	0.3	1.0

* Displacements corresponding to the distorted conformations X_i^- of Fig. 3. Modes 7 and 11 expose Orn^{3}H; mode 9 exposes Orn^{2}H.
† Angles in degrees.
‡ Angstroms.

and mode 11, respectively. For the β wag that exposes Orn^3 (mode 7) atoms of Gly^2 located in the middle of the β turn move as much as 4 Å (Fig. 3, $X_7^{\pm}$); in contrast, all of the backbone atoms move <1 Å along the path that exposes Orn^2H (Fig. 3, $X_9^{\pm}$).

Intramolecular hydrogen bonds in ferrichrome must be ruptured if hydrogen exchange of bonded protons is to occur. It is of interest to compare the intramolecular hydrogen bond geometries in the equilibrium conformation with their values along the exposure paths. The hydrogen bond $H \cdots O$ distances and $N—H \cdots O$ angles of the energy minimized structure and the distorted conformations of Fig. 3 are listed in Table 2. Weakening of the hydrogen bond is necessary for exposure of the corresponding amide proton. Along mode 7, the β wag breaks the $Orn^3H \cdots O$ Gly^2 hydrogen bond by increasing both the $H \cdots O$ distance and $N—H \cdots O$ angle ($\Delta R = 1.70$ Å; $\Delta\theta = 70°$, for the distorted geometry Fig. 3, X_7). For mode 11 the same hydrogen bond is distorted to a smaller extent ($\Delta R = 0.90$ Å; $\Delta\theta = 40°$). The Orn^2H exposure path involves primarily a stretching distortion of the hydrogen bond ($\Delta R = 0.62$ Å; $\Delta\theta = 12°$, Fig. 3, X_9). Of the three exposure paths studied in detail, two (modes 9 and 11) selectively break the hydrogen bond of the exposed proton while the other peptide hydrogen bonds remain intact. For example, along mode 9, which exposes Orn^2H, the adjacent Orn^3 hydrogen bond remains very close to the optimal value ($\Delta R = 0.06$ Å; $\Delta\theta = 12°$, Table 2). The highly selective nature of hydrogen bond cleavage observed for these exchange paths is in contrast to proposed mechanisms that involve unfolding for which cooperative breaking of adjacent hydrogen bonds is likely to be important (1, 5).

The ultimate goal of theoretical studies of hydrogen exchange in biopolymers is to provide a molecular interpretation for experimentally observed exchange rates and to establish the connection between molecular dynamics and hydrogen exchange. The complete theoretical evaluation of rate constants for hydrogen exchange in ferrichrome must involve: (i) molecular mechanics studies of peptide strain leading to solvent contact; (ii) quantum mechanical studies of the potential surface for proton transfer; and (iii) the evaluation of exchange rate constants with analytic or trajectory methods. Although work on the quantitative evaluation of hydrogen exchange rate constants for ferrichrome is not yet complete, a qualitative comparison of our present results with experimentally determined hydrogen exchange rate constants can be made. The rate constants for exchange of the four sterically blocked protons have

been measured at pH 3.14, pH 5, and pH 7. At the low pH, the chelated metal ion that maintains the native structure is competitively displaced by protonation of the carbamoylated side chains and hydrogen exchange of all of the peptide protons approaches the free peptide rate. As the pH is raised the stability of the native structure is increased so that the smaller normal mode deformations are likely to provide the most important exchange paths at pH 7. The sterically blocked protons exchange at neutral pH with rate constants $Gly^3 > Orn^3 > Orn^2 > Orn^1$. Considering first the slowest exchanging proton, Orn^1, from our normal mode analysis we conclude that local fluctuations about the native structure do not expose this proton to solvent so that exchange of Orn^1 must occur via gross molecular unfolding. The (EX 1) exchange behavior of this proton is explained by this conclusion (10, 21). In contrast, we have identified normal mode paths for exposure of Orn^2, Orn^3, and Gly^3. Gly^3 is already largely exposed in the native structure and there are at least 10 normal mode paths that increase its solvent accessibility. The exchange rates of Orn^2 and Orn^3 lie between the Orn^1 and Gly^3 values, with Orn^2 exchanging slower than Orn^3. Both protons are totally shielded from solvent in the native structure. That the β wag at 18 cm^{-1} provides a more efficient path for solvent contact of Orn^3 than paths that expose Orn^2 may explain the relative exchange rates for these two protons. Finally, because the β turn is a common structural unit in many peptides and proteins (22), several features of the exposure paths described here may also be important for exchange in biopolymers that incorporate a similar structural design.

Table 2. Hydrogen bond geometry*

	$^RH \cdots O^\dagger$	$^\theta N—H \cdots O^\ddagger$
Equilibrium		
$Orn^3H \cdots O$ Gly^3	1.94	11
$Orn^2H \cdots Oz$ Orn^2	1.90	23
Mode 7		
$Orn^3H \cdots O$ Gly^3	3.64	78
$Orn^2H \cdots Oz$ Orn^2	2.45	28
Mode 9		
$Orn^3H \cdots O$ Gly^3	1.98	5
$Orn^2H \cdots Oz$ Orn^2	2.52	35
Mode 11		
$Orn^3H \cdots O$ Gly^3	2.98	63
$Orn^2H \cdots Oz$ Orn^2	2.17	37

* Displacements corresponding to the distorted conformations of Fig. 2. Modes 7 and 11 expose Orn^3H; mode 9 exposes Orn^2H.
† Angstroms.
‡ Degrees.

1. Englander, S. W., Downer, N. W. & Teitlebaum, H. (1972) *Annu. Rev. Biochem.* **41**, 903–923.
2. Woodward, C. K. & Hilton, B. D. (1979) *Annu. Rev. Biophys. Bioeng.* **8**, 99–127.
3. Wuthrich, K., Wagner, G., Richarz, R. & Braun, W. (1980) *Biophys. J.* **32**, 549–560.
4. Wedin, R., Delepierre, M., Dobson, C. M. & Poulsen, F. (1982) *Biochemistry* **21**, 1098–1103.
5. Englander, S. W., Calhoun, D. B., Englander, J. J., Kallenbach, N. R., Liem, R. K. H., Malin, E. L., Mandal, C. & Rogero, J. R. (1980) *Biophys. J.* **32**, 577–589.
6. Richards, F. M. (1979) *Carlsberg Res. Commun.* **44**, 47–72.
7. Woodward, C. K. & Hilton, B. D. (1980) *Biophys. J.* **32**, 561–575.
8. Kossiakoff, A. A. (1982) *Nature (London)* **296**, 713–721.
9. Wlodawer, A. & Lennart, S. (1982) *Proc. Natl. Acad. Sci. USA* **79**, 1418–1422.
10. Emery, T. (1967) *Biochemistry* **6**, 3858–3866.
11. Llinas, M., Klein, M. & Neilands, J. B. (1973) *J. Biol. Chem.* **248**, 915–923.
12. Llinas, M., Klein, M. & Neilands, J. B. (1973) *J. Biol. Chem.* **248**, 924–931.
13. Gō, M. & Gō, N. (1976) *Biopolymers* **15**, 1119–1127.
14. Levy, R. M. & Karplus, M. (1979) *Biopolymers* **18**, 2465–2495.
15. Levy, R. M., Perahia, D. & Karplus, M. (1982) *Proc. Natl. Acad. Sci. USA* **79**, 1346–1350.
16. Noguti, T. & Gō, N. (1982) *Nature (London)* **296**, 776–778.
17. Gelin, B. R. & Karplus, M. (1979) *Biochemistry* **18**, 1256–1268.
18. Van der Helm, D., Baker, J. R., Eng-Wilmot, D. L., Hossain, M. B. & Loghry, R. A. (1980) *J. Am. Chem. Soc.* **102**, 4224–4231.
19. Richards, F. M. (1977) *Annu. Rev. Biophys. Bioeng.* **6**, 151–176.
20. Salemme, F. R. (1982) *Nature (London)* **299**, 754–755.
21. Englander, S. W. & Kallenbach, N. R. *Q. Rev. Biophys.*, in press.
22. Smith, J. A. & Pease, L. G. (1980) *CRC Crit. Rev. Biochem.* **8**, 315–400.